A Proposition for Improving the Design of Motor Windings for Low-Pressure Environment

Daniel Roger, Sonia Ait-Amar, Ewa Napieralska-Juszczak, Piotr Napieralski

A Proposition for Improving the Design of Motor Windings for Low-Pressure Environment

Daniel Roger, *Senior Member, IEEE,* Sonia Ait-Amar, *Member, IEEE,* Ewa Napieralska, *Senior Member, IEEE,* and Piotr Napieralski, *Senior Member, IEEE,*

***Abstract*—A new approach is proposed for designing coils free of partial discharges (PDs) for compact machines operating at high altitudes. The proposed method consists in using an enameled wire made with a thin additional resistive layer on the outer surface , which reduces strongly the electrical field in the voids between the wires of random coils. With such a wire, PDs occur only in specific zones situated near the wire connections and a local reinforcement of the insulation can increase strongly the partial discharge inception voltage (PDIV). The paper proposes a theoretical method for determining the properties of the resistive layer. The local reinforcement of the insulation is analysed with an electrostatic simulation and Paschen's law. Measurements confirm the effectiveness of the proposed method.**

***Index Terms*—Resistive layer, Electrical machine windings, Aircraft environment, Partial Discharge Inception Voltage (PDIV), Paschen's law.**

I. Introduction

In more electric aircrafts, the electrical energy brings many advantages comparing to hydraulic and pneumatic ones. For increasing the electric power with the same copper wire mass, the aircraft industry uses higher and higher voltages, switching from 115V ac to 540V dc. Studies are under progress for designing aircrafts with an electrical assistance during take off, requiring higher voltage grids [1]–[3]. Generally speaking, high power density electric actuators are connected to the dc grid by inverters that provide an efficient machine control and power reversibility. However, the electronic switches of inverters impose steep-fronted voltage pulses causing repetitive high magnitude short voltage spikes that stress the machine insulation. These problems were detected more than two decades ago when IGBT converters spread in industry [4], [5]. These spikes may cause PDs in the small remaining air-voids in the machine coils. It is now known that the space charges trapped in the polymer layers makes the analysis more complex [6]. Measurement method of the Partial Discharge Inception Voltage (PDIV) inside low voltage machines has been developed [7], [8]. PDs cause an earlier aging of the Electrical Insulation System (EIS) [9]–[12]. These problems are more critical at low pressures because PDs appear at lower voltages [13], [14].

Many machine topologies can be used in aircraft motors and generators [15], [16]. A solution consists in using prefabricated coils with a careful design of the turn deterministic arrangement for keeping the turn-to-turn voltage stress under the PDIV everywhere in the machine [17]. An estimation of the PDIV can be made using 2D electrostatic simulations and Paschen's law [18]. This coil technology can only be applied to permanent magnet synchronous machines (PMSM) or synchronous reluctant machines (SRM) made with concentrated windings and opened slots (one coil per stator tooth). With such prefabricated coils, the slot filling factor is lower than for standard random coils directly wound in the stator slots.

For compact machines that require a high slot feeling factor, the random winding method is better. The exact position of each turn remains unknown. The probability to have the input turn near the output one is not negligible [19]; the turn-to-turn voltage may be large and PDs may appear.

A solution consists in accepting a reasonable number of PDs during the whole expected life time of the machine using corona resistant wires. This enameled wire is made with an external polymer layer charged with micro or nano hard particles of inorganic materials that resist to PD abrasion [20]–[22].

Our research shows that another approach can be used; it consists in adding a thin resistive layer on the outer surface of enameled wire. This layer changes the electric field distribution in the EIS. It concentrates the field in the thin polymer layer of the enameled wire, which can withstand high field strengths. For a voltage stress over the PDIV, PDs appears only in specific zone situated near the end-connections of the coil which can easily be reinforced. Some of these issues were presented at the ITEC 2018 conference in California [23]. The paper proposes an extension of the theoretical approach for estimating the resistivity of this layer able to reduce the voltage turn-to-turn stress, with limited extra losses inside the additional resistive layers. The paper uses a standard compact machine design for defining the electrical properties of the resistive layer that can be easily added by enameled wire manufacturers without changing the external diameter. Experiments are performed on twisted pairs and random coils made with a wire covered with a resistive paint. They prove the effectiveness of the proposed principle before convincing an enameled wire manufacturer to test the new wire.

II. Environment of Aircraft Electrical Machines

For studying PDs in aircraft embedded machines, it is necessary to consider temperature and pressure in the small remaining air-voids between the enameled wires of the machine coils. Several cases are possible: the motor can be

D. Roger, S. Ait-Amar and E. Napieralska are in the Artois University (EA4025), Laboratoire Systèmes Electrotechniques et Environnement (LSEE) 62400, Bethune, France.

P. Napieralski is in the Institute of Information Technology, Lodz University of Technology, ul. Stefanowskiego 18/22, 90-924 Lodz, Poland.

placed inside the cabin, where the air-control system provides classical temperatures and pressures (80% of the sea-level pressure). For this case, the motor operating conditions are very near the classical ones and no specific investigations are necessary.

For electrical machines placed outside the cabin, two cases must be analysed: the air-void can be a closed bubble without any contact with the air outside the machine (closed air-void) or a small volume open towards the outside atmosphere (open air-void). For the first case, the air pressure inside the closed air-void does not depend on the ambient pressure but only of the temperature. For the second case, the air-void pressure is equal to the ambient one at the considered altitude, which can be estimated by the standard atmosphere table [24] giving temperatures and pressures at any point in the world .

The pressure in closed air-void, depends on the machine manufacturing process. A varnish always impregnates machine windings.Whatever the impregnation process, it ends by a polymerization thermal cycle in an oven. At the beginning of this cycle, the varnish is liquid. When the temperature increases, the closed air-void volume changes for getting a global pressure balance. During the polymerization process at a constant temperature, the varnish viscosity increase slowly. At the end of the polymerization, the varnish is a hard thermoplastic material, the volume of the closed air voids does not change anymore.When the temperature of the oven decreases, the pressure in the constant volume void decreases following the perfect gas law.

Table I gives 3 typical altitudes and the corresponding temperature and pressures in open and closed air-voids.

TABLE I
TEMPERATURES AND PRESSURES IN THE AIR-VOIDS OF A MACHINE PLACED OUTSIDE THE CABIN.

Alt. (m)	Alt. (feet)	Temp. (^{o}C)	Open v. (hPa)	Close v. (hPa)
0	0	15	1013	738
5000	16404	-17.5	541	658
10000	32808	-50	265	574

Paschen's formulae (1), based on Townsend's gas ionization theory [25], can be used for getting an estimation of the electronic avalanche threshold voltage V_{Th} between the air-void border that create an ionization of the air. It results of experimental works on ionization of a gas, at a given pressure p, placed between two flat electrodes at a distance d. This expression yields the threshold voltage from the pressure distance product (pd). For dry air at 20^oC, $B = 365\ V.Torr^{-1}.cm^{-1}$. C is defined by (2) where $A = 15\ Torr^{-1}.cm^{-1}$; γ is the second Townsend coefficient $\gamma \approx 0.01$ for polymer.

$$V_{Th} = \frac{B\ (p.d)}{C + \ln((p.d)} \tag{1}$$

$$C = ln\Big\{\frac{A}{1 + 1/\gamma}\Big\} \tag{2}$$

The correction (3) considers the gas density at a given temperature improves the Paschen's law [26]. In (3), V_{Th0} is the Paschen's threshold voltage computed at room temperature ($20^oC, 293^oK$); the pressure p is expressed in Torr ($760\ Torr = 1013\ hPa$).

$$V_{Th}(p,T) = \frac{293}{T}\ \frac{p}{760}\ V_{Th0}(p.d) \tag{3}$$

Figure 1 shows the Paschen's curves for the 3 temperatures of table I. The horizontal axis is the pd product with standard units. For instance, the vertical dotted line at $pd = 0.1\ hPa.m$ corresponds to an air-void thickness $d \approx 100\ \mu m$ and a sea-level pressure ($p = 1013\ hPa$). For this case, the Partial Discharge Inception Voltage (PDIV) is about $850\ V$ at 15^oC. It slightly increases at low temperatures.

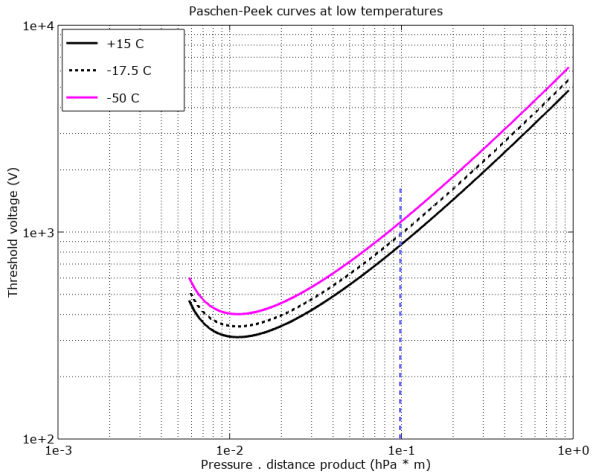

Fig. 1. Paschen's threshold voltage in air versus distance d between flat parallel electrodes for the 3 temperatures of table I.

Let us remind that Paschen's experiences were made with uniform fields. In a motor winding aircois, the electric field is not uniform. A more detailed analysis of Paschen's hypothesis shows that, at sea-level pressure, Paschen's law can be used with a reasonable error when the Pashen's distance d is replaced by the length of the part of the electric field lines in air-voids [27].

Recent experimental works confirm the Paschen's law for distances and pressure over the Paschen's minimum [28]–[30]. Another recent work confirms the Peek's correction for very cold Nitrogen [31].

III. DRAWBACK OF PDS IN MACHINE WINDINGS AND PROPOSED IMPROVEMENT

The most widely used enameled wires are made with two polymers. The polyester-imide (PEI) in contact with the copper provides a good adherence. The polyamide-imide (PAI) provides the required mechanical and thermal properties. The global thicknesses of the insulating layers is defined in the IEC 60317 standard [32]; it depends on the wire diameter and its grade.

The enameled wire is manufactured with a complex industrial process, which consists in depositing many thin layers of $\simeq 3\ \mu m$ that are polymerized separately in an oven. This operation is repeated 10-15 times for getting the insulating

thickness defined by the standards. With this manufacturing process, no significant air-void can exist inside the insulation layer of the enameled wire. Since the polymer has a much higher breakdown electric field than air, PDs occur in the air voids between wires. PDs cause a slow erosion polymer insulation layer. Figure 2 shows a microscopy of the cross-section of a twisted pair made of standard enameled wire eroded by many PDs. The abrasion near the contact point is clearly visible. The phenomena are similar with corona-resistant enameled wire but the abrasion is much slower; the time before failure is much longer [20].

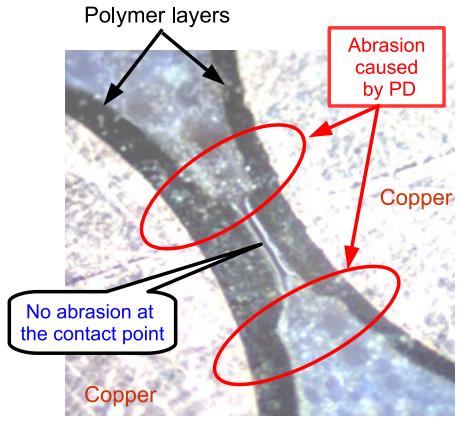

Fig. 2. Microscopy of the cross section of a twisted pair aged by a strong PD activity where the polymer layer abrasion is visible.

IV. Motor coil made with an enameled wire coated by a resistive layer

A. Example of compact machine

Compact machine are very often made with round enameled copper wire and random coils. For high currents, coils are wound with several small wires in hand. They are placed in the slots by their opening. This winding technology is used with semi-closed slots that reduce the cogging torque. Let us consider a compact 3-phase 12-teeth 10-pole PMSM widely used in more electric aircrafts for cabin pressurisation systems. For this example, the air-gap diameter is 80 mm, the stator length is also 80 mm. This machine is made with 12 coils, one per stator tooth. The rated values are: 8000 rpm; 400 V_{RMS}; 25 A_{RMS} and 17 kW.

In each slot, polymer sheets provide the common mode insulation and the insulation between the two coils. The 3 phases are made of 4 coils connected in series with the appropriate connections for producing a 10-pole rotating field. Each coil is made of 20 turns wound with 5 enameled wires of diameter 1 mm in hand. For such coils, the probability to have a wire of the input turn adjacent to a wire of the output one is large.

The turn-to-turn insulation must be designed for this worst case. In a more electric aircrafts, the inverters connected to the 540 V on-board dc bus feed the machines; their EISs must be designed considering the electrical stresses due to the inverter fast fronted voltages.

Our proposition consist in changing the varnish bath of the last layers of the enameled wire manufacturing process, using PAI charged with micro particles of carbon, for getting a thin resistive outer layer. The theoretical approach is aimed at defining a method able to find the suitable resistivity of the outer resistive layer. The influence of this layer on the machine insulation analysed considering the two adjacent wires presented in figure 3.

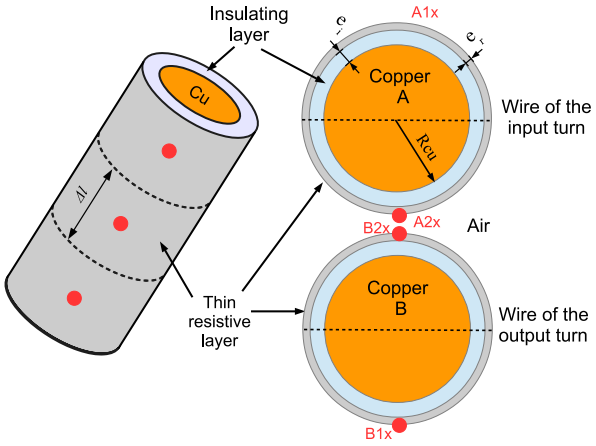

Fig. 3. Enameled wire with its external resistive layer and transversal section of two adjacent wires.

B. General assumptions and simplifications

The theoretical analysis of the influence of the outer resistive layer is made considering several assumptions:
- PDs may appear only in the residual air bubbles between the outer resistive layers of the wires.
- The study is made for the worst case in a random winding made of turns with several round wires in hand. A wire of the input turn is supposed to be adjacent to a wire or the output turn.
- The Y-connected machine is fed by a PWM inverter with fast fronted voltages. The first coil of each phase is supposed to withstand the full voltage stress during the fast transients.
- Only short times ($< 1\mu s$) corresponding to fast transients are considered. The complete study of the transients in the machine and the feeding cable is out of the scope: the Ph-N voltage waveform is an input data.
- The analysis uses the equivalent circuit presented in figure 4. This circuit is based on a regular mesh of the two resistive layers of adjacent wires. Each resistive layer is cut in a set of half cylinders of length $\Delta l = 2.5\ mm$ as presented in the left part of figure 3. The red points $A1x$, $A2x$, $B1x$, and $B2x$ are placed at the centre of the half cylinders, they corresponds yo the x^{th} column of the equivalent circuit of figure 4.
- The insulating and the resistive layers are supposed to be perfect cylinders of constant thicknesses made of homogenous and isotrope materials. Their sizes are used for computing the resistance and the capacitances of the equivalent circuit of figure 4. The capacitances between the copper and the resistive layer ΔC_W are drawn in black. The capacitances between the resistive layers ΔC_S are drawn in green; they

are estimated to $\Delta C_W/10$. This value is estimated form capacitance measurements on twisted pairs.
- For a random winding in a slot, the resistive outer layers of adjacent wires are in contact in limited number of points because the wires are not perfectly straight. Several simulations have been made for understanding the influence of the number of contact points between adjacent wires and their resistances. As expected, the voltage stress in the air between wires is all the weaker as the contacts are numerous and their resistances small. A pessimistic case is considered with only 8 contact points on the length of a stator slot (10 mm between contacts), with a resistance ΔR_S equal to the longitudinal resistance between the centre of two consecutive half cylinder ΔR_L.
- The simulation of the electric field in the connection zone of a wire is made in 2D with linear conditions. The additional hypothesis are explained in section IV-D.

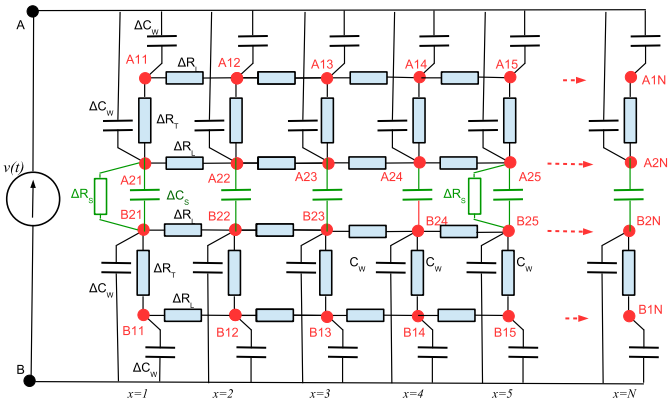

Fig. 4. Equivalent HF circuit able to estimate the voltage stress in the air between the wires with a SPICE processor.

C. Maximum voltage stress between adjacent wires of a coil

The voltage stress are computed with the equivalent circuit of figure 4 with a Spice processor. The parameters are estimated considering the wire sizes ($R_{CU} = 0.5mm$; a polymer layer of 30 μm and a resistive one of 6 μm). The polymer relative permittivity is $\epsilon_R = 3.5$. The resistive layer resistivity is $\rho = 10.10^{-3}\Omega.m$. For these values $\Delta R_L = 396\ \Omega$, $\Delta R_T = 560\ \Omega$ and $\Delta C_W = 4.2\ pF$.

The input voltage $v(t)$ is representative of a transient state observed on the Ph-to-N voltage of a machine connected to an inverter with a 4-meter long cable; the voltage spike is 550 V.

Considering the pessimistic case define above, the peak voltage stress on the air layer is only 100 V, which is under the Paschen minimum at low pressures of the airliner flying altitude. With more contact points between the resistive layers, the peak voltage stress is lower. The peak voltage is located halfway between two contact points.

For a motor coil made with the proposed enameled wire, the resistive layers in contact together form closed loops around each stator tooth that create eddy currents and additional losses.

The global resistance of such a close loop is computed for the worst case that suppose a perfect contact between the external surface of wires. All the resistive layers of a coil are connected in parallel (one resistance per wire, 5 wires per turn, 20 turns = 100 resistances connected in parallel). For each coil this closed resistive loop creates extra Joule losses that are estimated to 32 W per coil for the motor steady state at its rates power.

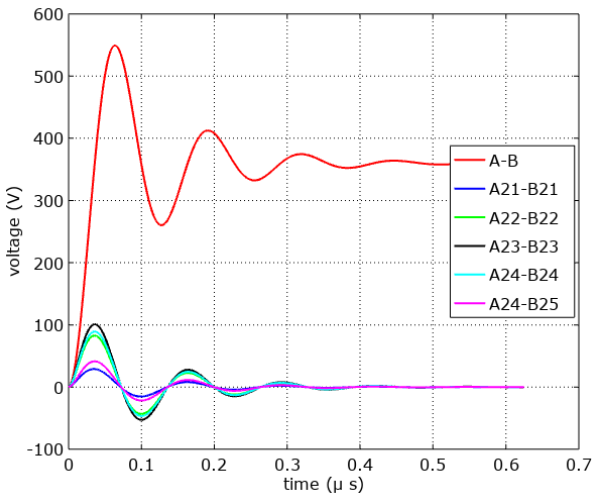

Fig. 5. Voltage between several points of the adjacent wire resistive layers.

It is well known that the voltage stress due to the inverter fast fronted voltages is concentrated on the first turns of the first coils of each phase. For the other coils, the common-mode capacitances mitigate the voltage spikes. Only the first coil of each phase should use the proposed solution; the other ones can be wound with a standard enameled wire without any resistive layer . The additional losses estimation is 128 W, which represents only 0.75% of the motor rated power.

D. Finite element simulation in the connection zones

A special care must be paid in the vicinity of the coil end-connections: the outer resistive layer must be stopped far form the nude copper wire as shown in figure 6. Consequently, a high electric field exists in the air of this specific zone and PDs appear.

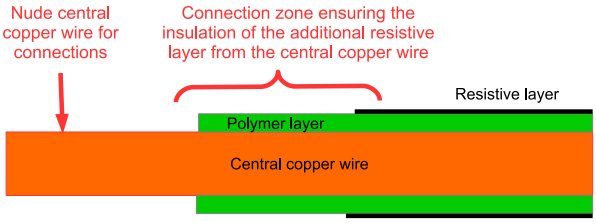

Fig. 6. Longitudinal section of the end-connection of the enameled wire with an external resistive layer. A specific zone with a high electric field appears.

The electric field is computed in the polymer and in the ambient air using a 2D finite-element (FE) software. The mesh is built at the micrometer scale (figure 7). The exact shape of the external conducting layer is supposed to be smooth. The field is computed in linear conditions with a constant polymer

relative permittivity of 3.5 and for 1 kV imposed between the resistive layer and central copper wire. The simulation results can be applied to other voltages because of the problem linearity.

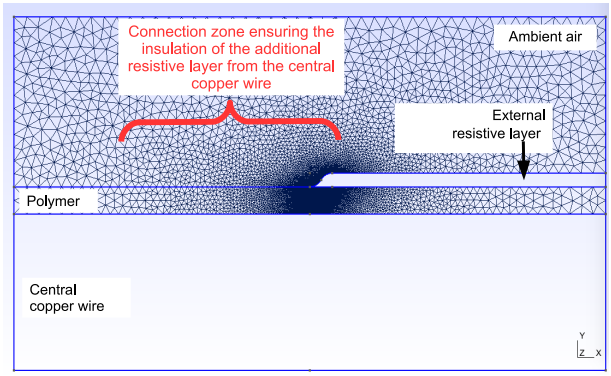

Fig. 7. 2D mesh of the air and polymer in the specific zones at the end of the external conducting layer.

The FE simulation yields the field lines of figure 8. They are plotted in the air of the specific zone near the connections. PDs may occur in the air but not in the polymer because of its higher dielectric strength. The numbers added at the bottom of each line is a simple serial number, from the longest line to the shortest one.

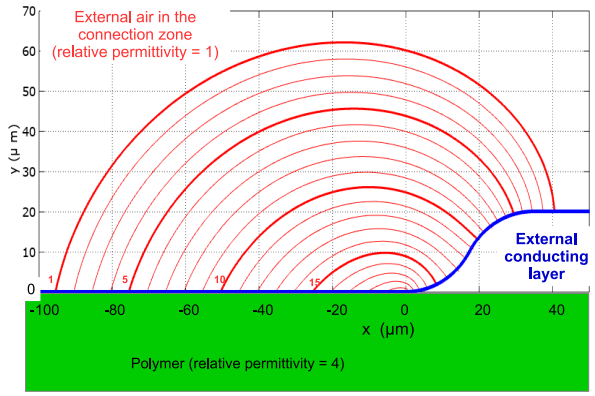

Fig. 8. Field lines in the air of the connection zone.

The global shape of these field lines is far from the straight lines of the uniform field of the Paschen's theory. A deeper analysis must be made before applying Paschen's results.

Let us remind that Paschen's works were mainly based on the Townsend's gas ionization theory [25] and on a free electrons accelerated by the Coulomb's force. This theory is valid only before ionization for estimating the voltage threshold of the electronic avalanche. Following Townsend's theory, an electronic avalanche appears when an accelerated free electron acquires enough energy for ionizing a gas molecules when a collision occurs. After the electronic avalanche ignition, the development and extinction of PDs require more complex analysis based on plasma theory. The PDIV corresponds to the voltage at the very beginning of the electronic avalanche. In Paschen's theory, the free electrons are accelerated following the straight field lines: the speed ($\vec{v}$) and the Coulomb force ($\vec{F}$) are collinear vectors. The free electron trajectories are straight lines superimposed with the field lines, which have the same length d.

With a non-uniform field, free electrons do not follow exactly the field lines because their mass influence the trajectories. The proposed analysis adds the inertial equation due to the electron mass m. The input data is the force field $\vec{F} = q\vec{E}$ defined by a square mesh, which is 0.5 μm. The electric field $\vec{E}$ is computed in air, with the FE simulation described above. The hypothesis are similar to Townsend's and Paschen's ones based on a mechanical interpretation of the physical phenomena in gas:

- The electronic avalanche is a succession of ionizing collisions of gas molecules by accelerated free electrons.
- When the applied voltage is exactly equal to the electronic avalanche ignition voltage, the changes in the local field due to ions are not considered.
- When an accelerated free electron collides an atom of a gas molecule with enough energy, the atom absorbs the kinetic energy for creating a new free electron at zero speed.
- The air of the connection zone is only composed of molecule that ionization energy is 14 eV (this value is 14.5 eV for Nitrogen and 13.6 eV for oxygen).
- Elastic collisions and thermal agitation are not considered.

The mechanical time differential equation is simulated with Euler method and a very short time step (0.01 ps) because of the low value of the electron mass (10^{-30} kg). Each trajectory is computed using a starting point defined at zero speed $\vec{v} = \vec{0}$ at the beginning point of a field line situated on the border between polymer and air. Figure 9 considers two starting points at the beginning of field lines 10 and 15 in figure 8. For each time step the free electron speed ($\vec{v}$) and the kinetic energy $w = \frac{1}{2}m|\vec{v}|^2$ are computed. An ionizing collision is supposed to occur when this kinetic energy is $14eV$, which initialize the speed to $\vec{v} = \vec{0}$ at the current position represented by a small circle in Figure 9. The trajectory ends when it reaches the external resistive layer. The script computes also the trajectory length.

Figure 9 shows that, for the considered geometry and the given voltage, the free electron trajectories (black lines) are very close to the corresponding field lines (red lines). It is not exactly the case for a lower voltage (green lines) estimated to 1/3 of the previous voltage. The first voltage corresponds to the PDIV at sea-level pressure; the second one correspond to the PDIV at an airliner flying altitude. The distance between two successive ionizing collisions is larger because of the lower Coulomb accelerating force. The trajectory and field line lengths are compared in table II.

TABLE II
COMPARISON OF TRAJECTORIES AND FIELD LINES LENGTH.

Field line Nb.	Field line length (μm)	Tr. length for 625 V (μm)	Diff. (%)	Tr. length for 210 V (μm)	Diff. (%)
10	84.3	84.8	0.6	88	4.3
15	40	40	0	41	2.5

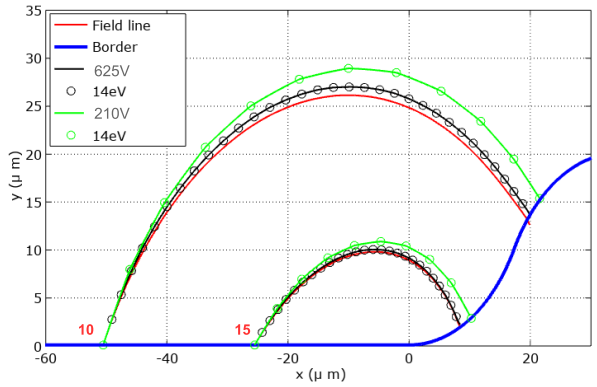

Fig. 9. Field lines in the air of the connection zone.

For starting points situated at the beginning of a longer field line, the curves are similar but the acceleration is weaker; the distance between two ionizing collisions is larger and the difference between the field line length and the trajectory one is a bit larger. Accepting an error under 10%, the field line lines length can be used instead successive free electrons trajectories one for estimating the threshold voltage of an electronic avalanche in the specific connection zones.

Figure 10 presents the Paschen's curves for the 3 altitudes of Table I and the FE simulation results. The horizontal axis is the length of the field lines in the external air of the specific connection zone. Each red $+$ sign is associated with the field line number defined in figure 8. The FE simulation is made with a constant permittivity for each material: the electric field modulus at any point of the field map is proportional to the input voltage imposed to the copper wire. The field line positions and lengths (x-axis) remain the same whatever the input voltage. The potential difference between the ends of each field line (y-axis) is proportional to the input voltage. The red $+$ signs move up and down with the input voltage.

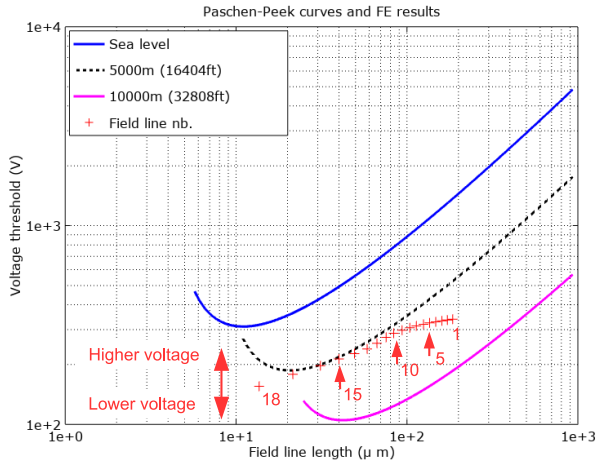

Fig. 10. FE results reported on the Paschen's curves.

In Figure 10, the red $+$ signs are drawn for an input voltage tuned to 650 V_{peak}. The voltage has been tuned for getting red points slightly under the Paschen's curve obtained for 5000 m. The very first electronic avalanches creating PDs appear along field lines $14-16$, which length are about 30 μm. At 10000 m and for the same voltage, the red $+$ signs are much over the Paschen's curve; many PDs exist. At sea-level pressure, the voltage can be higher (1300 V_{peak}) for getting $+$ signs on the Paschen's curve. PDs appear along shorter lines $17-18$.

V. Experimental verification of the concept validity

The experimental verifications were made on twisted pairs following the IEC 60172 standard [33] and placed in the frame of figure 11 for their immobilization. Samples 1,3,5 are made with a standard enameled wire; samples 2,4,6 are made with the same enameled wire covered with a black resistive paint that resistivity is 2750 $\mu\Omega.m$. The samples are hand-made and the actual paint thickness is not really known, but the experience is only aimed at verifying the principle. The PDIV and the PDs charges are measured using a wide spread commercial equipment.

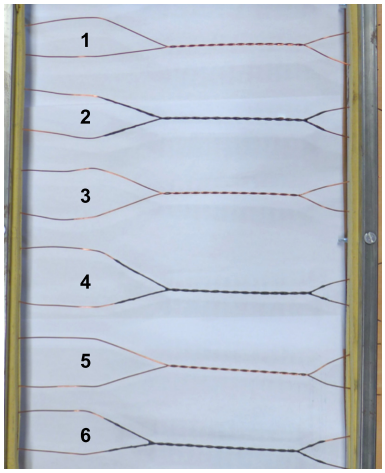

Fig. 11. Preparation of twisted pairs in a frame for their immobilization.

The PDIV is measured at $50Hz$ following the IEC 60270 standard [34], with a threshold of 5 pC at room temperature and pressure. The average value is 684 V_{RMS} for the specimens made with the standard enameled wire and 772 V_{RMS} for the wires covered with the resistive paint.

The twisted pairs of the frame were connected in parallel and fed by a voltage source at 50 Hz tuned at the double of the PDIV measured on standard samples for observing PDs. The frame was placed vertically in a dark cabinet and observed with a night vision camera called "Coronafinder" [35]. This system makes a visible image from UV radiations of PDs. Figure 12 presents the picture of samples 1-4. It can be seen that PDs exist along the body of the standard 1 and 3 and only at the ends of the resistive layers for samples 2 and 4. A similar experience has been made with small coils with classical wire of 0.85 mm diameter. Each coils in wound with two wires in hand and 20 turns. One of them is wound using wires covered with the same resistive paint. The same test bench has been used for electrical measurements and optical monitoring. The PDIVs are similar as those determined for the twisted pairs. For an applied voltage of 1500 V_{RMS} the PDs UV emission

are illustrated on figure 13 for both coils. PDs appear along the wire for the classical coil and only on the ends of the conducting paint layer for the second coil. The measured PDs apparent charge is 40 pC for the first coil and 25 pC for the second one.

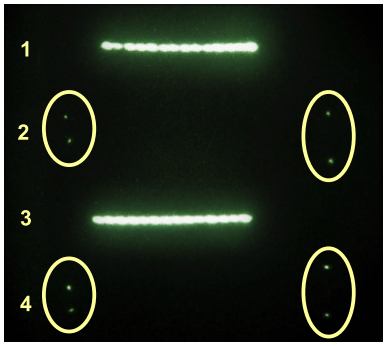

Fig. 12. Comparison of PDs activity. For samples made with a wire covered of conducting paint, the center of twisted pairs is free of PD; PDs appear only on the ends of the resistive layers.

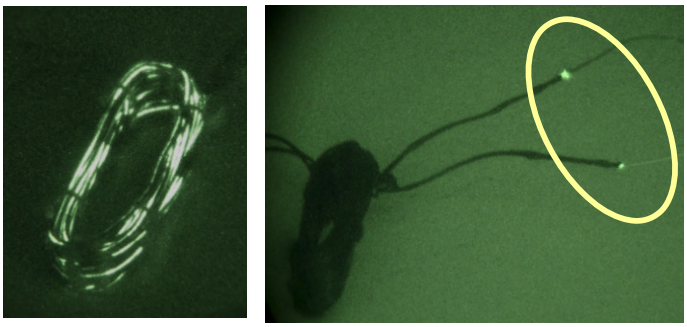

Fig. 13. Standard coil with a high voltage stress (left) and identical coil made with an enameled wire covered with a resistive paint (right).

A. Reinforcement of the specific zone where PDs may appear

For getting higher PDIV, it is possible to add a varnish drop at the end on the external conducting layer. A 2D FE simulation explains this effect considering an example of varnish drop represented in 2D by a 40 μm radius circle. The varnish relative permittivity is supposed to be the same as the polymer; the mesh remains the same. Figure 14 presents the field lines in air and in the polymer drop for the same starting points as in figure 10. It can be seen that the relative permittivity of the polymer drop extends the field lines.

Figure 15 presents Paschen's curves at 3 altitudes. The red circles correspond to the field lines in air drawn in figure 14 (length and potential difference between their ends). It can be seen that the electronic avalanche initiating PDs, at an altitude of 10000 m, is obtained for the longest field lines 1-3 corresponding to higher potential differences between their ends.

The PDIV depends on the polymer drop geometry: for a bigger polymer drop, the red circles are shifted down. The contact with Paschen's curve is obtained for longer field lines that corresponds to higher potential differences between their ends.

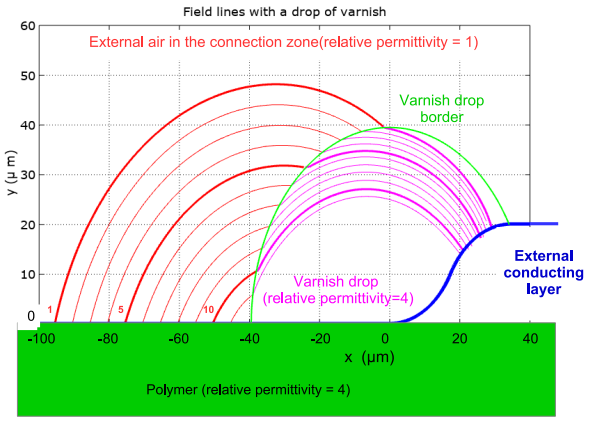

Fig. 14. Field lines in the reinforced connection zone.

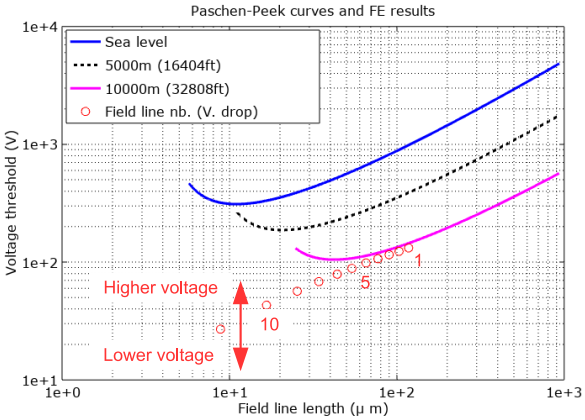

Fig. 15. FE results reported on the Paschen's curves.

VI. Conclusion

A new approach for designing the windings of compact PMSM fed by PWM inverters, free of partial discharges at high altitudes is proposed. The method consists of adding a thin resistive layer on the outer surface of the enameled wire used to built the first coil of each phase. In a random coil, the multiple contacts between the external resistive layers reduce strongly the electrical field in the residual air-voids existing between wires. With the external resistive layer, PDs appear in specific zones situated near the wire connections. It is possible to reduce strongly the PDs activity in these zones by adding small quantities of varnish at the end of the resistive layer.

After studying the environment of electrical machines embedded in aircrafts, the influence of pressure and temperature on the PDIV is explained. Then, the influence of the outer resistive layer of the proposed new enameled wire is explained in detail, considering a compact motor design. The proposed analysis is made with a HF equivalent circuit and a Spice processor that reproduces the fast transient voltage measured on a motor fed by a PWM inverter. This analysis shows that the contact points number between wires ant their resistances have a major influence on the voltage stress in the residual air voids between wires. A very pessimist case of the random winding is considered. It shows that a reasonable

resistivity of 20.10^{-3} $\Omega.m$ (more than $100,000$ times the copper one) brings interesting results with a voltage spikes under the Paschen's minimum. This external resistive layer concentrates the electric field in the polymer of the enameled wire. Consequently, PDs appears in very small zones near the connections.

FE simulations of such a specific zone show that the classical Paschen's law can be used for estimating the PDIV with an error under 10%. They show also that the PDIV can be increased by adding a polymer drop in the small zones near the connections.

Experimental verifications using an wire covered with a resistive paint, have been made with twisted pairs and random coils. They confirm the validity of the concept. The electrical properties of the resistive layer are now defined. Works in progress concerns the industrial development of the new enameled wire compatible with the thermal and mechanical requirement of compact motor design.

REFERENCES

[1] D. Zhang, J. He, D. Pan, M. Dame, and M. Schutten, "Development of megawatt-scale medium-voltage high efficiency high power density power converters for aircraft hybrid-electric propulsion systems," in *2018 AIAA/IEEE Electric Aircraft Technologies Symposium (EATS)*, July 2018, pp. 1–5.

[2] J. Thauvin, G. Barraud, X. Roboam, B. Sareni, M. Budinger, and D. Leray, "Hybrid propulsion for regional aircraft: A comparative analysis based on energy efficiency," in *2016 International Conference on Electrical Systems for Aircraft, Railway, Ship Propulsion and Road Vehicles International Transportation Electrification Conference (ESARS-ITEC)*, Nov 2016, pp. 1–6.

[3] J. Chen, C. Wang, and J. Chen, "Investigation on the selection of a more suitable power system architecture for future more electric aircraft from the prospective of system stability," in *2017 IEEE 26th International Symposium on Industrial Electronics (ISIE)*, June 2017, pp. 1861–1867.

[4] S. Bell and J. Sung, "Will your motor insulation survive a new adjustable-frequency drive?" *Industry Applications, IEEE Transactions on*, vol. 33, no. 5, pp. 1307–1311, Sep 1997.

[5] L. Manz, "Motor insulation system quality for IGBT drives," *IEEE Industry Applications Magazine*, vol. 3, no. 1, pp. 51–55, Jan 1997.

[6] M. E. Banda, D. Malec, and J.-P. Cambronne, "Simulation of space charge impact on partial discharge inception voltage in power busbars dedicated to future hybrid aircrafts," *Scientific Research Publishing*, 2018.

[7] D. Bogh, J. Coffee, G. Stone, and J. Custodio, "Partial-discharge-inception testing on low-voltage motors," *IEEE Transactions on Industry Applications*, vol. 42, no. 1, pp. 148–154, Jan 2006.

[8] C. Abadie, T. Billard, and T. Lebey, "Partial discharges in motor fed by inverter: From detection to winding configuration," *IEEE Transactions on Industry Applications*, vol. 55, no. 2, pp. 1332–1341, March 2019.

[9] P. Maussion, A. Picot, M. Chabert, and D. Malec, "Lifespan and aging modeling methods for insulation systems in electrical machines: A survey," in *2015 IEEE Workshop on Electrical Machines Design, Control and Diagnosis (WEMDCD)*, March 2015, pp. 279–288.

[10] N. Lahoud, J. Faucher, D. Malec, and P. Maussion, "Electrical aging of the insulation of low-voltage machines: Model definition and test with the design of experiments," *IEEE Transactions on Industrial Electronics*, vol. 60, no. 9, pp. 4147–4155, Sept 2013.

[11] D. Fabiani, G. C. Montanari, and A. Contin, "Aging acceleration of insulating materials for electrical machine windings supplied by pwm in the presence and in the absence of partial discharges," in *Solid Dielectrics, 2001. ICSD '01. Proceedings of the 2001 IEEE 7th International Conference on*, 2001, pp. 283–286.

[12] D. Barater, F. Immovilli, A. Soldati, G. Buticchi, G. Franceschini, C. Gerada, and M. Galea, "Multistress characterization of fault mechanisms in aerospace electric actuators," *IEEE Transactions on Industry Applications*, vol. 53, no. 2, pp. 1106–1115, March 2017.

[13] L. Lusuardi and A. Cavallini, "The problem of altitude when qualifying the insulating system of actuators for more electrical aircraft," in *2018 IEEE International Conference on Electrical Systems for Aircraft, Railway, Ship Propulsion and Road Vehicles International Transportation Electrification Conference (ESARS-ITEC)*, Nov 2018, pp. 1–4.

[14] F. Koliatene, T. Lebey, J.-P. Cambronne, and S. Dinculescu, "Impact of the aeronautic environment on the partial discharges ignition: A basic study," in *Electrical Insulation, 2008. ISEI 2008. Conference Record of the 2008 IEEE International Symposium on*, June 2008, pp. 603–606.

[15] W. Cao, B. Mecrow, G. Atkinson, J. Bennett, and D. Atkinson, "Overview of electric motor technologies used for more electric aircraft (mea)," *Industrial Electronics, IEEE Transactions on*, vol. 59, no. 9, pp. 3523–3531, Sept 2012.

[16] Y. Jia and K. Rajashekara, "An induction generator-based ac/dc hybrid electric power generation system for more electric aircraft," *IEEE Transactions on Industry Applications*, vol. 53, no. 3, pp. 2485–2494, May 2017.

[17] V. Iosif, S. Duchesne, and D. Roger, "Voltage stress predetermination for long-life design of windings for electric actuators in aircrafts," in *2015 IEEE Conference on Electrical Insulation and Dielectric Phenomena (CEIDP)*, Oct 2015, pp. 318–321.

[18] S. Duchesne, G. Parent, J. Moenecley, and D. Roger, "Prediction of pdiv in motor coils using finite element method," in *2016 IEEE International Conference on Dielectrics (ICD)*, vol. 2, July 2016, pp. 638–641.

[19] S. Duchesne, V. Mihaila, G. Vélu, and D. Roger, "Study of wire distribution in a slot of a motor fed by steep fronted pulses for lifetime extension," in *IEEE International Symposium on Electrical Insulation ISEI - San Juan (USA)*, 2012, pp. 601–605.

[20] A. Cavallini, M. Conti, D. Fabiani, and G. Montanari, "Evaluation of corona-resistant magnet wires through partial discharge and space charge measurements," in *Electrical Insulation Conference and Electrical Manufacturing amp; Coil Winding Conference, 2001. Proceedings*, 2001, pp. 11–16.

[21] C. Hudon, N. Amyot, and J. Jean, "Long term behavior of corona resistant insulation compared to standard insulation of magnet wire," in *Electrical Insulation, 2000. Conference Record of the 2000 IEEE International Symposium on*, 2000, pp. 13–16.

[22] A. T. Honag, "Electrical characterization of partial discharge resistant enamel insulation," *Memoire High Voltage Engineering Department of Materials and Manufacturing Technology Chalmers University of Technology SE-41296 Gothenburg Sweden*, 2013.

[23] D. Roger, S. Ait-Amar, E. Napieralska, and P. Napieralski, "A proposition for improving the design of motor windings for low-pressure environment," in *2018 IEEE Transportation Electrification Conference and Expo (ITEC)*, June 2018, pp. 424–429.

[24] Public Domain Aeronautical Software (PDAS), "Properties of the U.S. standard atmosphere," *http://www.pdas.com/atmosTable1US.html.*, 1976.

[25] J. S. Townsend, *The theory of ionization of gases by collision*. Constable & Company LTD, 1910.

[26] IEC 60060-1, "High voltage measurement techniques part 1," *International Electrotechnics Commission*, 1989.

[27] D. Roger, S. Ait-Amar, and E. Napieralska, "A method to reduce partial discharges in motor windings fed by PWM inverter," *Open Physics,*, vol. 16, no. 1, pp. 599–604, 2018.

[28] N. Allen, M. Abdel-Salam, and I. Cotton, "Effects of temperature and pressure change on positive corona and sparkover under direct voltage in short airgaps," *IET Science Measurement Technology*, 2007.

[29] P. Osmokrovic, "Mechanism of electrical breakdown of gases at very low pressure and interelectrode gap values," *IEEE Transactions on Plasma Science*, vol. 21, no. 6, pp. 645–653, Dec 1993.

[30] E. Sili, J. P. Cambronne, and F. Koliatene, "Temperature dependence of electrical breakdown mechanism on the left of the paschen minimum," *IEEE Transactions on Plasma Science*, vol. 39, no. 11, pp. 3173–3179, Nov 2011.

[31] R. Massarczyk, P. Chu, C. Dugger, S. Elliott, K. Rielage, and W. Xu, "Paschen's law studies in cold gases," *Journal of Instrumentation*, vol. 12, no. 06, p. P06019, June 2017. [Online]. Available: http://stacks.iop.org/1748-0221/12/i=06/a=P06019

[32] IEC 60317-0-1, "Specifications for particular types of winding wires - part 0-1: General requirements - enamelled round copper wire," 2013.

[33] IEC 60172, *Test procedures for the determination of the temperature index of enameled and tape wrapped winding wires*, International Electrotechnics Commission Std., 2015.

[34] IEC 60270, *High-voltage test techniques, partial discharge measurements*, International Electrotechnics Commission Std., 2001.

[35] Syntronics, "UV direct view system coronafinder." [Online]. Available: http://syntronics.net/coronafinder.html